Available online at www.sciencedirect.com
ScienceDirect
Journal of Sound and Vibration 297 (2006) 664–679
JOURNAL OF SOUND AND VIBRATION
www.elsevier.com/locate/jsvi

A fixed–free interface component mode synthesis method for rotordynamic analysis

A. Shanmugam, Chandramouli Padmanabhan*

Machine Design Section, Department of Mechanical Engineering, Indian Institute of Technology Madras, Chennai 600036, India

Received 13 September 2004; received in revised form 6 April 2006; accepted 17 April 2006
Available online 21 June 2006

Abstract

A fixed–free interface component mode synthesis method has been developed for carrying out rotordynamic analysis with the gyroscopic effects being considered. This hybrid model has been developed to combine the advantages of the fixed interface method, known popularly as the Craig–Bampton approach and the free interface method, known as the Craig–Chang technique. It is shown in the paper that the proposed fixed-free interface method is able to predict the whirl frequencies accurately (like the Craig–Bampton method) and at the same time predict the unbalance response accurately (like the Craig–Chang approach). The proposed technique has been validated for two systems. (a) a cantilever rotor with a heavy disc at its free end and (b) a typical twin-spool aero-engine rotor-bearing configuration. This technique is also suitable for nonlinear analysis, when a squeeze film damper is present.

1. Introduction

Rotor dynamic analysis is a complex task particularly when it is carried out on a rotor-bearing system such as multi-spool rotors of aero-engines, which have two or more rotors spinning coaxially and supported on comparatively flexible supporting case structure. Additional features to be included in the analysis, as compared to conventional structural dynamic analysis, are the gyroscopic effects due to the precession of rotors, which makes the analysis complex due to its influence on the natural frequencies of the rotor system. In addition, the size of the problem is a cause of concern for the analyst when transient analysis is to be considered.

The development of an aero-engine is a multidisciplinary task and many of its components are developed simultaneously by different departments, which carry out respective dynamic analysis of their components. Thus the wealth of data available with the concerned divisions from the dynamic analyses carried out by them on individual components cannot be utilized, if the entire rotor-bearing-casing system is analyzed at once.

In order to address and overcome all the above challenges, the component mode synthesis (CMS) is a natural choice for the rotor dynamics analyst. CMS enables analysis to be carried out on different individual components by various departments with necessary reduction of problem size at each stage either using modal

*Corresponding author.
E-mail address: mouli@iitm.ac.in (C. Padmanabhan).

0022-460X/$ - see front matter
doi:10.1016/j.jsv.2006.04.011

Nomenclature

$[A]$, $[B]$ state matrices
$[C]$, $[E]$ constraint and elastic flexibility matrices
$\{p\}$, $\{q\}$ generalized coordinates vector, independent generalized coordinates vector
I_p polar moment of inertia of the rotor component
L, T, V lagrangian, kinetic and strain energy
$\{f\}$, $\{u\}$, $\{\dot{u}\}$ force, displacement and velocity vectors
$[P]$, $[R]$ mode acceleration and reaction force matrices
$[S]$ selection matrix
$[m]$, $[g]$, $[k]$ mass, gyroscopic and stiffness matrices
$[t]$ transformation matrix
$\{y\}$ state-space vector of displacement and velocity
$[\Phi]$ modal matrix of component with boundary degrees-of-freedom fixed
$[\Lambda]$ diagonal matrix of eigenvalues of component with boundary degrees-of-freedom fixed
$[\Psi_a]$, $[\Psi_c]$ constraint mode matrix, attachment mode matrix
$\{\sigma\}$ lagrange multipliers vector

Subscripts

ii, *ij*, *ji*, *jj* interior–interior, interior–boundary, boundary–interior, boundary–boundary partitions
i, *j* interior and boundary degrees-of-freedom
d, *l* dependent and independent generalized coordinates
dd, *dl* dependent–dependent, dependent–independent partitions of constraint matrix
wa, *ra*,*aa* complementary, rigid-body and attachment coordinates

Superscripts

r component index
1, 2 sub-rotor 1 and 2 for example case

displacement or mode acceleration methods and build a final model of highly reduced size. This also enables the analyst to perform corrective or design modifications at the component level to achieve desired dynamic behavior without having to wait for the analysis of the final system. This reduces the number of design iterations.

A good review by Nelson [1] is available on various modal reduction techniques including CMS developed for rotordynamic analysis. Comparative analysis of all modal synthesis techniques, such as CMS, branch mode analysis, component mode substitution and coupled free–free component modes, developed for dynamic analysis of large structures has been reported. Hurty et al. [2] recommend the fixed–fixed CMS of Craig and Bampton as the most trustworthy method for all vibration analyses. The Craig and Bampton [3] method was originally developed for structural dynamics by Hurty [4]. The Craig and Bampton method gives a more accurate eigensolution for a given number of component modes. Craig and Chang [5] developed a free interface CMS, in which the residual attachment modes were used to account for the flexibility of all modes. This method has been shown to produce better results when applied to structures having large number of attachment or boundary coordinates. Li and Gunter [6] have successfully applied free interface CMS to large rotor systems. However in this method, interconnecting elements are modeled as linear elastic elements and added to the final formulation using normal modes. Glasgow and Nelson [7] have extended the fixed interface CMS method to examine the stability of rotor systems.

In this paper, fixed–free interface CMS has been developed for rotordynamic analysis, including the gyroscopic effect. This hybrid method combines the advantages of the Craig and Bampton [3] and Craig and Chang [5] approaches. In this method, the final reduced equations of motion are obtained using Lagrange's equations based on Lagrange multipliers to incorporate constraint equations. The given rotor is divided into sub-rotors and the boundary coordinates attached to one sub-rotor are fixed and corresponding boundary coordinates attached to adjoining sub-rotor are free. Normal modes obtained, based only on the inertia and stiffness matrices of sub-rotors, are used for modal reduction of all sub-rotor matrices including the gyroscopic matrix. In order to verify the accuracy of results of whirl frequencies, which are spin dependent due

to the gyroscopic effect, a cantilever beam with a heavy disc at the free end is considered. This example is considered as the gyroscopic effect will be significant. This rotor has been analyzed for whirl frequencies using a full model finite element method (FEM). These results are compared with the results obtained from CMS using normal modes based only on the inertia and stiffness matrices. Further, results are also obtained using Meirovitch [8] formulation, in which the modal matrix for modal truncation is obtained at every spin speed due to the presence of the gyroscopic matrix.

After this validation, the above rotor has been analyzed for both whirl frequency and unbalance response using fixed–free interface methods and the results obtained are compared with the results obtained using full finite element model, fixed interface (Craig and Bampton) and free interface (Craig and Chang) methods. Finally, the present method has been applied to a typical twin-spool aero-engine model and the results once again compared with the results obtained using full finite element model, Craig and Bampton and Craig and Chang methods. In this model, the inter-shaft bearing used to couple both the rotors is modeled as an elastic member and forms part of the low pressure (LP) sub-rotor, whose coordinates are retained as physical coordinates, so that any nonlinear mechanism such as SFD associated with these coordinates could be analyzed later in isolation to the system linear coordinates, which is one of the attractive features of this present formulation.

2. Fixed–free CMS formulation for rotordynamics

In this formulation, the junction coordinates attached to one component are fixed and corresponding junction coordinates attached to the other component are free. The modes involved in this formulation are basically classified into normal modes, constraint modes and attachment modes.

The equation of undamped motion of a rotor system is given by

$$[m]\{\ddot{u}(t)\} - \mathbf{\Omega}[g]\{\dot{u}(t)\} + [k]\{u(t)\} = \{f(t)\}, \tag{1}$$

where $[m]$, $[g]$, $[k]$, $\{u(t)\}$and $\{f(t)\}$ are the mass, gyroscopic and stiffness matrices, displacement and force vectors, respectively, with $\mathbf{\Omega}$ being the rotor angular speed. The given system is divided into many sub-systems/components, whose coordinates are partitioned into interior $\{u_i\}$ and boundary or junction coordinates $\{u_j\}$ as given by

$$\{u\}^{\mathrm{T}} = \begin{bmatrix} \{u_i\}^{\mathrm{T}} & \{u_j\}^{\mathrm{T}} \end{bmatrix}. \tag{2}$$

The junction coordinates are shared with other substructures. Accordingly the equation of motion of a component is expressed in the partitioned form as

$$\begin{bmatrix} [m_{ii}] & [m_{ij}] \\ [m_{ji}] & [m_{jj}] \end{bmatrix} \begin{Bmatrix} \{\ddot{u}_i\} \\ \{\ddot{u}_j\} \end{Bmatrix} - \mathbf{\Omega} \begin{bmatrix} [g_{ii}] & [g_{ij}] \\ [g_{ji}] & [g_{jj}] \end{bmatrix} \begin{Bmatrix} \{\dot{u}_i\} \\ \{\dot{u}_j\} \end{Bmatrix} + \begin{bmatrix} [k_{ii}] & [k_{ij}] \\ [k_{ji}] & [k_{jj}] \end{bmatrix} \begin{Bmatrix} \{u_i\} \\ \{u_j\} \end{Bmatrix} = \begin{Bmatrix} \{f_i\} \\ \{f_j\} \end{Bmatrix}. \tag{3}$$

If the component is completely constrained at its junctions, only interior degrees-of-freedom (dof) are participating in the eigenvalue analysis. Therefore Eq. (3) can be expressed in terms of interior coordinates as:

$$[m_{ii}]\{\ddot{u}_i\} - \mathbf{\Omega}[g_{ii}]\{\dot{u}_i\} + [k_{ii}]\{u_i\} = \{0\}. \tag{4}$$

Expressing the above equation in first-order form using state-space vector $\{y\}^{\mathrm{T}} = \begin{bmatrix} \{\dot{u}_i\} & \{u_i\} \end{bmatrix}^{\mathrm{T}}$ one gets

$$[A]\{\dot{y}\} + [B]\{y\} = \{0\}, \quad A = \begin{bmatrix} [m_{ii}] & [0] \\ [0] & [k_{ii}] \end{bmatrix}, \quad B = \begin{bmatrix} [g_{ii}] & [k_{ii}] \\ -[k_{ii}] & [0] \end{bmatrix}. \tag{5}$$

The above equation needs to be solved for every spin speed to obtain state vectors, which is a computationally intensive effort. In order to overcome this, one assumes that the state vectors or eigenvectors do not appreciably change with rotor spin speed. The validity of this assumption will be demonstrated later using a

simple cantilever beam with a heavy disc at its free end. In this system the gyroscopic effects are usually quite significant. In general, Eq. (2) can be transformed as

$$\{u\}^r = [t]^r \{p\}^r, \tag{6}$$

where $[t]^r$ is the transformation matrix and $\{p\}^r$ is the vector of generalized coordinates for the rth component, with $r = 1,2,\ldots,n$. The system equations of motion are obtained using Lagrange's equation with Lagrange multipliers,$\{\sigma\}$, to enforce the constraint equations. The constraint equations are as follows:

$$\{u\}_j^1 = \{u\}_j^2 = \ldots = \{u\}_j^r \tag{7}$$

which in matrix form can be written as

$$[C]\{p\} = \{0\}. \tag{8}$$

The Lagrangian for the system is then given by

$$L = T - V + \{\sigma\}^{\mathrm{T}}[C]\{p\}, \tag{9}$$

where the kinetic energy T and strain energy V of the system are obtained by summing the kinetic and strain energies of all the components [9].

$$T = \sum_{r=1}^{n}\left(\frac{1}{2}\{\dot{u}\}^{r\mathrm{T}}[m]^r\{\dot{u}\}^r - \frac{1}{2}\mathbf{\Omega}\{\dot{u}\}^{r\mathrm{T}}[g]^r\{u\}^r + \frac{1}{2}I_P\mathbf{\Omega}^2\right), \quad V = \sum_{r=1}^{n}\frac{1}{2}\{u\}^{r\mathrm{T}}[k]^r\{u\}^r. \tag{10}$$

Substituting Eq. (6) into Eq. (10), one gets T and V in the generalized coordinates and substituting these into Eq. (9), yields

$$\begin{aligned} L = \sum_{r=1}^{n}\Bigg(&\frac{1}{2}\{\dot{p}\}^{r\mathrm{T}}[t]^{r\mathrm{T}}[m]^r[t]^r\{\dot{p}\}^r - \frac{1}{2}\mathbf{\Omega}\{\dot{p}\}^{r\mathrm{T}}[t]^{r\mathrm{T}}[g]^r[t]^r\{p\}^r + \frac{1}{2}I_P\mathbf{\Omega}^2 \\ &- \frac{1}{2}\{p\}^{r\mathrm{T}}[t]^{r\mathrm{T}}[k]^r[t]^r\{p\}^r + \{\sigma\}^{r\mathrm{T}}[C]^r\{p\}^r\Bigg). \end{aligned} \tag{11}$$

The above equation is reduced and expressed for the whole system as

$$L = \frac{1}{2}\{\dot{p}\}^{\mathrm{T}}[M]\{\dot{p}\} - \frac{1}{2}\mathbf{\Omega}\{\dot{p}\}^{\mathrm{T}}[G]\{p\} + \frac{1}{2}I_P\mathbf{\Omega}^2 - \frac{1}{2}\{p\}^{\mathrm{T}}[K]\{p\} + \{\sigma\}^{\mathrm{T}}[C]\{p\}. \tag{12}$$

The system equations of motion can now be obtained using Lagrange's equation:

$$\frac{\mathrm{d}}{\mathrm{d}t}\left(\frac{\partial L}{\partial \dot{p}_s}\right) - \frac{\partial L}{\partial p_s} = Q_s. \tag{13}$$

Differentiating Eq. (12) with respect to $\{\dot{p}\}$ and then differentiating with respect to time, t, yields for the entire system:

$$\frac{\partial L}{\partial\{\dot{p}\}} = [M]\{\dot{p}\} - \frac{1}{2}\mathbf{\Omega}[G]\{p\}, \quad \frac{\mathrm{d}}{\mathrm{d}t}\left(\frac{\partial L}{\partial \dot{p}}\right) = [M]\{\ddot{p}\} - \frac{1}{2}\mathbf{\Omega}[G]\{\dot{p}\}. \tag{14}$$

Differentiating Eq. (12) with respect to $\{p\}$, yields:

$$\frac{\partial L}{\partial\{p\}} = -\frac{1}{2}\mathbf{\Omega}[G]^{\mathrm{T}}\{\dot{p}\} - [K]\{p\} + [C]^{\mathrm{T}}\{\sigma\}. \tag{15}$$

Substituting Eqs.(14) and (15) into Eq. (13), one gets

$$[M]\{\ddot{p}\} - \mathbf{\Omega}[G]\{\dot{p}\} + [K]\{p\} = [C]^{\mathrm{T}}\{\sigma\} + [t]^{\mathrm{T}}[f]. \tag{16}$$

Let $\{p\}$ be partitioned into dependent coordinates $\{p_d\}$ and independent co-ordinates $\{p_l\}$, which will be retained in the final formulation, and substituting into Eq. (8), one gets

$$\begin{bmatrix}[C_{dl}] & [C_{dd}]\end{bmatrix}\begin{Bmatrix} p_l \\ p_d \end{Bmatrix} = \{0\}, \quad \{p_d\} = -[C_{dd}]^{-1}[C_{dl}]\{p_l\}, \quad \{p_l\} = \{q\}. \tag{17}$$

Eq. (17) can be used to rewrite Eq. (8) as

$$[C]\begin{bmatrix} I_{ll} \\ -C_{dd}^{-1}C_{dl} \end{bmatrix}\{q\} = \{0\}, \quad [C][S]\{q\} = \{0\}. \tag{18}$$

Since $\{q\} \neq \{0\}$ this implies that

$$[C][S] = [0]. \tag{19}$$

Comparing Eq. (8) and (18), one gets

$$\{p\} = [S]\{q\}. \tag{20}$$

Substituting the above equation into Eq. (16) and pre-multiplying with $[S]^{\mathrm{T}}$ one gets

$$[S]^{\mathrm{T}}[M][S]\{\ddot{q}\} - \mathbf{\Omega}[S]^{\mathrm{T}}[G][S]\{\dot{q}\} + [S]^{\mathrm{T}}[K][S]\{q\} = [S]^{\mathrm{T}}[C]^{\mathrm{T}}\{\sigma\} + [S]^{\mathrm{T}}[t]^{\mathrm{T}}\{f\}. \tag{21}$$

Substituting Eq. (19) into Eq. (21), one gets the final reduced order equation of motion for a given system as

$$[M]_S\{\ddot{q}\} - \mathbf{\Omega}[G]_S\{\dot{q}\} + [k]_S\{q\} = [S]^{\mathrm{T}}[t]^{\mathrm{T}}\{f\} = \{F\}_S. \tag{22}$$

The above equation forms the basis for rotor dynamic analysis of rotor-bearing system.

2.1. Fixed boundary sub-rotor problem formulation

In this sub-rotor (rotor 1), the boundary or junction coordinates are fixed. The displacements of the interior coordinates are the summation of the displacements relative to fixed conditions at the junction, obtained from the mode shapes (with junctions fixed) and the displacements due to displacement of the junction points, included in the form of constraint modes. Normal modes are obtained from the eigenvalue analysis (symmetric matrices):

$$\left([k_{ii}^1] - \mathbf{\Omega}^2[m_{ii}^1]\right)[\mathbf{\Phi}] = [0]. \tag{23}$$

The modes are normalized with respect to mass and stiffness matrices to obtain

$$[\mathbf{\Phi}]^{\mathrm{T}}[m_{ii}^1][\mathbf{\Phi}] = I; \quad [\mathbf{\Phi}]^{\mathrm{T}}[k_{ii}^1][\mathbf{\Phi}] = \Lambda = \mathrm{diag}(\omega_n^2), \tag{24}$$

where $[\mathbf{\Phi}]$ is the modal matrix whose columns are the component normal modes and ω_n is the nth natural frequency. Further, the normal modes are truncated, including only the required numbers of modes in order to reduce the size of the problem without compromising on the accuracy of the results. The truncated set of normal modes is denoted by $[\mathbf{\Phi}_k]$ (kept normal modes) and is usually much smaller than the original number of modes.

A constraint mode is defined by statically imposing a unit displacement on one of the physical coordinates in the j set and zero displacement on the remaining coordinates (see Eq. (3)):

$$\begin{bmatrix} [k_{ii}^1] & [k_{ij}^1] \\ [k_{ji}^1] & [k_{jj}^1] \end{bmatrix}\begin{Bmatrix} [\mathbf{\Psi}_{ij}] \\ [I_{jj}] \end{Bmatrix} = \begin{Bmatrix} [0] \\ [f_{jj}] \end{Bmatrix}. \tag{25}$$

From the first row of the above equation one obtains $[\mathbf{\Psi}_{ij}] = -[k_{ii}^1]^{-1}[k_{ij}^1]$ and the constraint mode matrix is given by

$$[\mathbf{\Psi}_c] = \begin{Bmatrix} [\mathbf{\Psi}_{ij}] \\ [I_{jj}] \end{Bmatrix}. \tag{26}$$

Thus the displacement vector and reduced rotor sub-matrices can be expressed as:

$$\{u_i^1\} = [\Phi_k]\{p_i^1\} + [\Psi_c]\{p_j^1\}, \quad \begin{Bmatrix} \{u_i^1\} \\ \{u_j^1\} \end{Bmatrix} = \begin{bmatrix} [\Phi_{ik}] & [\Psi_{ij}] \\ 0 & [I_{jj}] \end{bmatrix} \begin{Bmatrix} \{p_i\} \\ \{p_j\} \end{Bmatrix} = [t^1]\{p^1\},$$

$$[k^{1s}] = [t^1]^{\mathrm{T}}[k^1][t^1], \quad [m^{1s}] = [t^1]^{\mathrm{T}}[m^1][t^1], \quad [g^{1s}] = [t^1]^{\mathrm{T}}[g^1][t^1]. \tag{27}$$

2.2. Free boundary sub-rotor problem formulation

The boundary coordinates of this sub-rotor (rotor 2) are kept free. In this formulation, the displacement transformation matrix comprises free interface normal modes and attachment modes with necessary restraint against rigid body motion. The stiffness matrix is divided into three sets, which are '*r*' (rigid body coordinates which provide restraint against rigid body motion), '*a*' (attachment or juncture coordinates) and '*w*' (complementary coordinates). The attachment modes $[\Psi_a]$ are defined by applying unit forces to the *a* set as given by

$$\begin{bmatrix} [k_{ww}^2] & [k_{wr}^2] & [k_{wa}^2] \\ [k_{rw}^2] & [k_{rr}^2] & [k_{ra}^2] \\ [k_{aw}^2] & [k_{or}^2] & [k_{oo}^2] \end{bmatrix} \begin{Bmatrix} [\Psi_{wa}] \\ [0_{ra}] \\ [\Psi_{aa}] \end{Bmatrix} = \begin{Bmatrix} [0_{wa}] \\ [R_{ra}] \\ [I_{aa}] \end{Bmatrix}, \quad [k^2][\Psi_a] = \{f\}. \tag{28}$$

Instead of attachment modes, inertia relief attachment modes are included based on the mode acceleration approach. Inclusion of the inertia relief attachment modes considerably improves the accuracy by accounting for the influence of the deleted modes. Residual attachment modes have been employed in CMS by Craig and Chang [5]. The sub-rotor is an unconstrained component and hence it needs residual inertia relief attachment modes in place of residual attachment modes.

Inertia relief modes are obtained by applying to a body an equilibrated load system $\{f_e\}$, which consists of the originally specified force vector $\{f\}$ equilibrated by the rigid body d'Alembert force vector $[m]^2\{\ddot{u}_r\}$, where $\{u_r\}$ is the rigid body motion due to $\{f\}$. The rigid body modes are obtained from the eigenvalue analysis of the unconstrained sub-rotor system and are normalized as

$$[\Psi_r]^{\mathrm{T}}[m^2][\Psi_r] = [I_{rr}]. \tag{29}$$

The equilibrated force is then obtained as

$$\{f\}_e = \{f\} - [m^2]\{\ddot{u}_r\} = [P]\{f\}, \quad [P] = [I] - [m][\Psi_r][\Psi_r]^{\mathrm{T}}. \tag{30}$$

Attachment modes $[\hat{\Psi}_a]$ relative to the *R* constraints then can be defined as

$$\begin{bmatrix} [k_{ww}^2] & [k_{wr}^2] & [k_{wa}^2] \\ [k_{rw}^2] & [k_{rr}^2] & [k_{ra}^2] \\ [k_{aw}^2] & [k_{ar}^2] & [k_{aa}^2] \end{bmatrix} \begin{Bmatrix} [\hat{\Psi}_{wa}] \\ [0_{ra}] \\ [\hat{\Psi}_{aa}] \end{Bmatrix} = \begin{bmatrix} [P_{ww}^2] & [P_{wr}^2] & [P_{wa}^2] \\ [P_{rw}^2] & [P_{rr}^2] & [P_{ra}^2] \\ [P_{aw}^2] & [P_{ar}^2] & [P_{aa}^2] \end{bmatrix} \begin{Bmatrix} [0_{wa}] \\ [0_{ra}] \\ [I_{aa}] \end{Bmatrix} = \quad [P^2]\{f\}. \tag{31}$$

Since the loads are equilibrated, there are no reactions at the *R* constraints. The rigid body modes are removed from $\hat{\Psi}_a$ by setting

$$[\Psi_a] = [\hat{\Psi}_a] + [\Psi_r]C_r, \quad [\Psi_r]^{\mathrm{T}}[m^2][\Psi_a] = [0]. \tag{32}$$

This will be satisfied if

$$[\Psi_a] = [P^2]^{\mathrm{T}}[\hat{\Psi}_a] = \left([P^2]^{\mathrm{T}}[E][P^2]\right)[F_a], \quad [E] = \begin{bmatrix} [g_{ww}] & [0] & [g_{wa}] \\ [0] & [0] & [0] \\ [g_{aw}] & 0 & [g_{aa}] \end{bmatrix}, \quad [F_a] = \begin{bmatrix} [0_{wa}] \\ [0_{ra}] \\ [I_{aa}] \end{bmatrix}. \tag{33}$$

However, if a complete set of free-interface modes were to be supplemented by attachment modes, the latter would be linearly dependent on the former and as such there is necessity to establish the attachment and normal modes as a set of linearly independent modes to satisfy the component synthesis process. This can be established as follows. Let the elastic normal modes be separated into kept modes $[\Gamma_k]$ and deleted modes $[\Gamma_d]$. Then the elastic flexibility matrix is given by

$$[E_e] = [E_k] + [E_d] = [P]^{\mathrm{T}}[E][P] = [\mathbf{\Gamma}_e][\Lambda_{ee}]^{\mathrm{T}}[\mathbf{\Gamma}_e]^{\mathrm{T}} = [\mathbf{\Gamma}_k][\Lambda_{kk}]^{-1}[\mathbf{\Gamma}_k]^{\mathrm{T}} + [\mathbf{\Gamma}_d][\Lambda_{dd}]^{-1}[\mathbf{\Gamma}_d]^{\mathrm{T}}. \tag{34}$$

From the above equation one can write as follows for the inertia relief modes:

$$[E_d] = [P]^T[E][P] - [\mathbf{\Phi}_k][\Lambda_{kk}]^{-1}[\mathbf{\Phi}_k]^T, \quad [\mathbf{\Psi}_d] = [E_d][F_a]. \tag{35}$$

The displacement transformation equation is now expressed in partitioned form as

$$\begin{Bmatrix} \{u_i^2\} \\ \{u_j^2\} \end{Bmatrix} = \begin{bmatrix} \mathbf{\Gamma}_{ik} & \mathbf{\Psi}_{id} \\ \mathbf{\Gamma}_{jk} & \mathbf{\Psi}_{jd} \end{bmatrix} \begin{Bmatrix} p_k^2 \\ p_d^2 \end{Bmatrix}, \quad \{u^2\} = [t^2]\{p^2\}. \tag{36}$$

The reduced sub-rotor 2 matrices are then given by

$$[k^{2s}] = [t^2]^{\mathrm{T}}[k^2][t^2], \quad [m^{2s}] = [t^2]^{\mathrm{T}}[m^2][t^2], \quad [g^{2s}] = [t^2]^{\mathrm{T}}[g^2][t^2]. \tag{37}$$

2.3. Synthesis of sub-rotors

The constraint eqation at the joining of the two rotors is that $\{u_j^1\} = \{u_j^2\}$. From Eq. (27) and (36), one obtains

$$\{u_j^1\} = \{p_j^1\}, \quad \{u_j^2\} = [\mathbf{\Gamma}_{jk}]\{p_k^2\} + [\mathbf{\Psi}_{jd}]\{p_d^2\}. \tag{38}$$

From the above equation and the constraint equation, $\{u_j^1\} = \{u_j^2\}$ the following expression can be derived:

$$\{p_d^2\} = \left[[\mathbf{\Psi}_{jd}]^{-1} - [\mathbf{\Psi}_{jd}]^{-1}[\mathbf{\Gamma}_{jk}] \right] \begin{Bmatrix} p_j^1 \\ p_k^2 \end{Bmatrix}. \tag{39}$$

The vector $\{p\}$ is further partitioned into independent and dependent coordinates, so that the dependent coordinates can be eliminated in the final formulation, leading to

$$\begin{bmatrix} C_{dl} & C_{dd} \end{bmatrix} \begin{Bmatrix} \begin{Bmatrix} \{p_i^1\} \\ \{p_j^1\} \\ \{p_k^2\} \end{Bmatrix} \\ \{p_d^2\} \end{Bmatrix} = \{0\}, \quad [C_{dl}] = \begin{bmatrix} [0] & [\mathbf{\Psi}_{jd}]^{-1} & -[\mathbf{\Psi}_{jd}]^{-1}[\mathbf{\Gamma}_{jk}] \end{bmatrix}, \quad [C_{dd}] = -[I]. \tag{40}$$

The final selection matrix $[S]$ is given by

$$[S] = \begin{bmatrix} [I] & 0 & 0 \\ [0] & [I] & [0] \\ [0] & [0] & [I] \\ [0] & [\mathbf{\Psi}_{jd}]^{-1} & -[\mathbf{\Psi}_{jd}]^{-1}[\mathbf{\Gamma}_{jk}] \end{bmatrix}. \tag{41}$$

Rearranging sub-rotor 1 and sub-rotor 2 matrices leads to the form

$$[K] = \begin{bmatrix} [k^1] & 0 \\ 0 & [k^2] \end{bmatrix}, \quad [M] = \begin{bmatrix} [m^1] & 0 \\ 0 & [m^2] \end{bmatrix}, \quad [G] = \begin{bmatrix} [g^1] & 0 \\ 0 & [g^2] \end{bmatrix}. \tag{42}$$

The final reduced system stiffness, mass and gyroscopic matrices are given by

$$[K_S] = [S]^T[K][S], \quad [M_S] = [S]^T[M][S], \quad [G_S] = [S]^T[G][S]. \tag{43}$$

In the next section two different rotor systems are analyzed using the procedure described above.

3. Results and discussion

The efficacy and superiority of the present method is demonstrated with two example rotors. The first rotor is of a cantilever type with a heavy disc fixed at its free end and the other end is supported on bearings, which is treated as a fixed support as shown in Fig. 1.

The heavy disc at the free end is used to generate considerable gyroscopic moments, so as to study its influence on the modal superposition method, in which the modal or transformation matrix, used to transform the system from physical to modal coordinates (with necessary truncation) has been evaluated without considering the gyroscopic matrix. This is to be compared with modal superposition method including the gyroscopic matrix. The second rotor is a typical twin-spool aero-engine rotor model, comprising lower pressure (LP) and high pressure (HP) spools rotating coaxially at different speeds with a speed ratio (HP/LP) of 1.5 and is shown in Fig. 2.

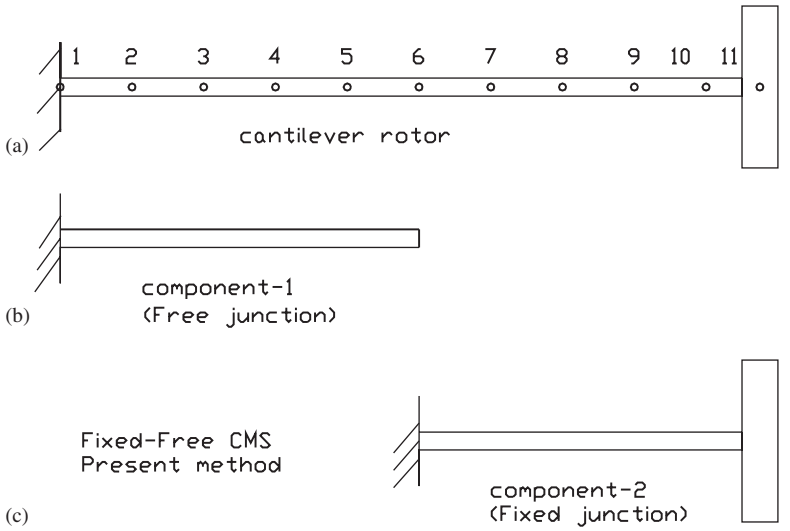

Fig. 1. Cantilever rotor model with total length of 2 m, the components, (a) full model, (b) component-1 with junction free and (c) component-2 with left junction fixed.

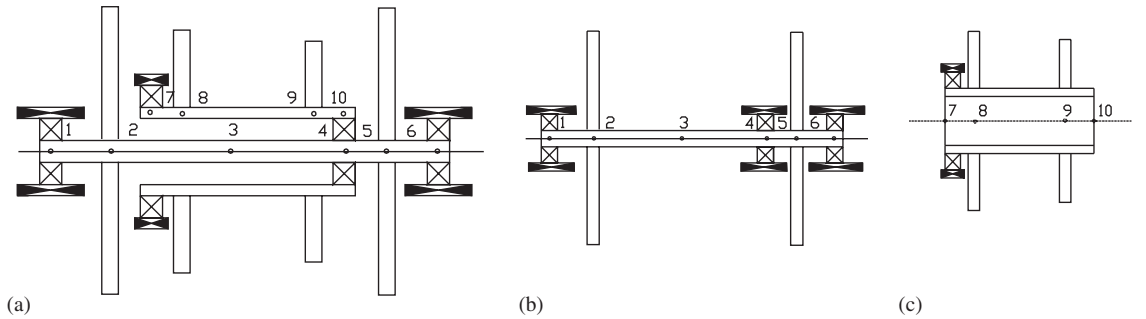

Fig. 2. A twin-spool aero-engine rotor model: (a) full schematic model, (b) LP rotor with junction fixed and (c) HP rotor with junction free.

Table 1
Comparison of whirl frequencies, in rad/s, at a rotor speed of 100,000 rev/min for the cantilever rotor shown in Fig. 1

Mode no.	Full FEM (40 modes)	Pseudo modal (20 modes)	Error %	Meirovitch (20 modes)	Error %
−1	1.3651e1	1.3651e1	6.8965e-4	1.3651e1	1.5858e-10
1	5.5263e1	5.5263e1	5.0555e-4	5.5263e1	4.7788e-9
−2	9.0467e1	9.0469e1	1.6066e-3	9.0467e1	5.5916e-9
2	4.1057e2	4.1057e2	1.1802e-3	4.1057e2	3.5137e-8
−3	4.7822e2	4.7823e2	2.0206e-3	4.7822e2	3.2210e-8
3	1.0868e3	1.0868e3	1.4802e-3	1.0868e3	6.2556e-8
−4	1.1908e3	1.1908e3	1.9335e-3	1.1908e3	6.7419e-8
4	2.0945e3	2.0945e3	1.3394e-3	2.0945e3	1.3406e-8
−5	2.2517e3	2.2518e3	2.3666e-3	2.2517e3	1.8350e-8
5	3.4344e3	3.4344e3	2.0585e-3	3.4344e3	9.4634e-9
−6	3.6635e3	3.6635e3	1.9298e-3	3.6635e3	1.2403e-8
6	5.1113e3	5.1114e3	1.8828e-3	5.1113e3	3.7910e-9
−7	5.4316e3	5.4317e3	2.7530e-3	5.4316e3	4.4814e-9
7	7.1337e3	7.1340e3	4.1506e-3	7.1337e3	5.0795e-9
−8	7.5657e3	7.5658e3	2.0043e-3	7.5657e3	5.8672e-9
8	9.5123e3	9.5128e3	5.5574e-3	9.5123e3	1.9828e-9
−9	1.0078e4	1.0079e4	3.5874e-3	1.0078e4	2.3536e-9
9	1.2240e4	1.2243e4	2.2721e-2	1.2240e4	1.0426e-7
−10	1.2968e4	1.2968e4	2.7821e-3	1.2968e4	1.0853e-7
10	1.5117e4	2.0155e4	3.3329e1	1.5117e4	4.6964e-9

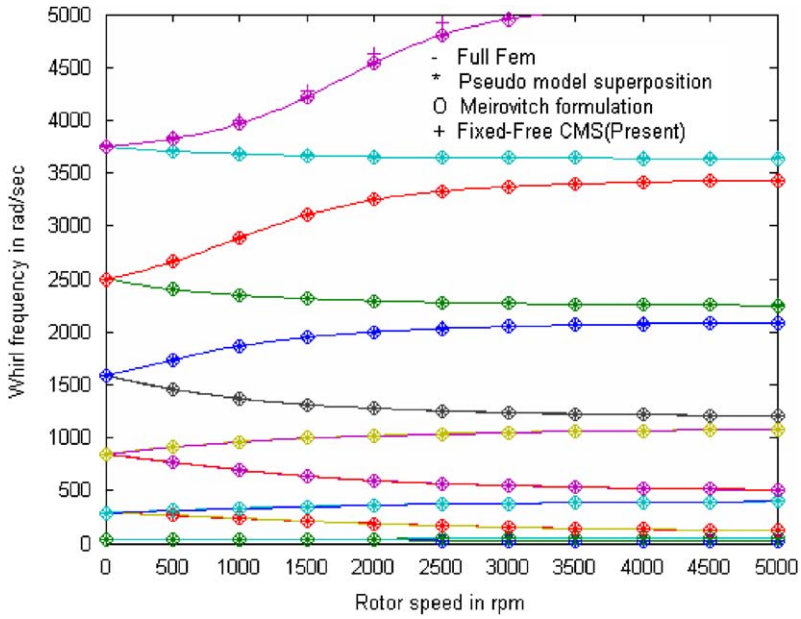

Fig. 3. Whirl frequency analysis of cantilever rotor with pseudo-modal and Meirovitch [8] method based calculation.

The first rotor has been analyzed for whirl speed using a full rotor model based on the FEM [9]. Beam elements with 4 dof at each node are used in the finite element formulation; there are a total of ten elements with 40 dof. This provides the bench mark for comparison with backward and forward whirl frequencies obtained using the CMS methods. The mass of the disc is 10 kg, the inside and outside diameters of the rotor are 25 and 50 mm, respectively, the polar moment of inertia and diametral moment of inertia of the disc are 0.2

Table 2
Comparative result of whirl frequencies, in rad/s, at a rotor speed of 50,000 rev/min for cantilever rotor (C–B, Craig and Bampton C–C, Craig and Chang)

Mode	Full FEM (40 dof)	Present (10 + 10)	% Error	C–B (10 + 10)	% Error	C–C (10 + 10)	% Error
−1	22	22	0	22	0	22	0
1	50	50	0	50	0	50	0
−2	118	118	0	118	0	118	0
2	395	395	0	395	0	396	0.252
−3	505	505	0	505	0	507	0.394
3	1074	1074	0	1074	0	1075	0.093
−4	1207	1207	0	1207	0	1209	0.165
4	2087	2087	0	2088	0.048	2079	0.384
−5	2250	2250	0	2251	0.044	2246	0.178
5	3433	3433	0	3435	0.058	3426	0.204
−6	3640	3640	0	3642	0.055	3630	0.275
6	5111	5113	0.039	5117	0.117	5157	0.892
−7	5382	5384	0.037	5389	0.130	5423	0.756
7	7106	7109	0.042	7112	0.084	7520	5.505
−8	7486	7489	0.040	7502	0.213	7768	3.630
8	9283	9292	0.090	9467	1.943	10,039	7.530
−9	9964	9977	0.130	10,068	1.033	10,915	8.712
9	10,807	10,820	0.120	10,902	0.871	11,162	3.180
−10	12,743	12,788	0.351	13,625	6.473	15,282	16.614
10	12,814	12,839	0.195	13,918	7.932	15,740	18.590

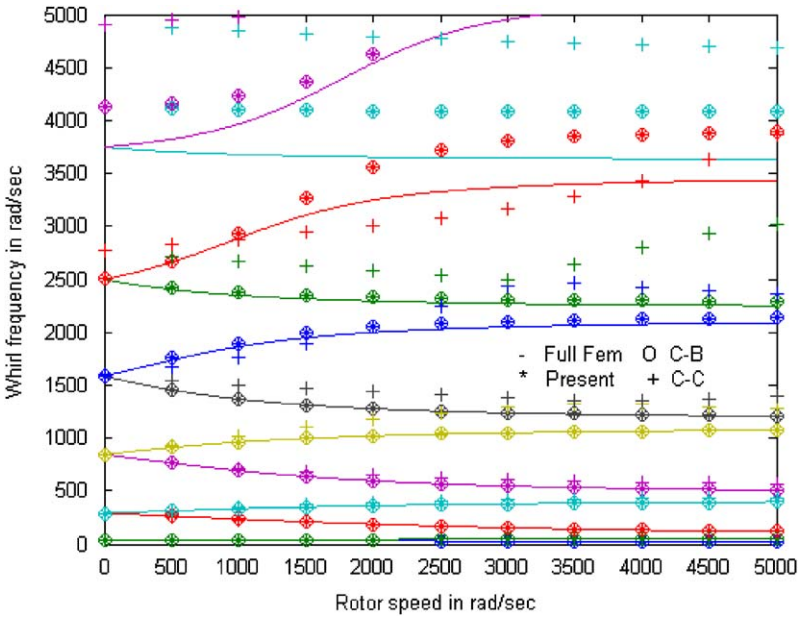

Fig. 4. Whirl frequency analysis of cantilever rotor with 30% of component modes (C–B, Craig–Bampton, C–C, Craig–Chang).

and 0.1 kg m^2, respectively. The results obtained are given in Table 1 and Fig. 3. It is observed from these results that whirl frequencies obtained using modal superposition method without the gyroscopic matrix (termed as pseudo-modal *n* the table) and the Meirovitch method [8] with gyroscopic matrix compare very well with the FEM result. To establish the effect of leaving out the gyroscopic matrix, a case was studied with a

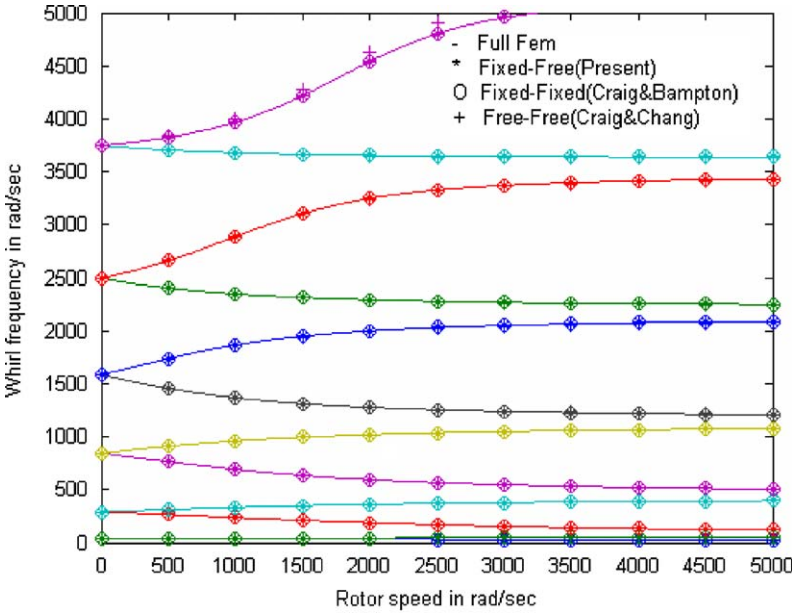

Fig. 5. Whirl frequency analysis of cantilever rotor with 50% component modes.

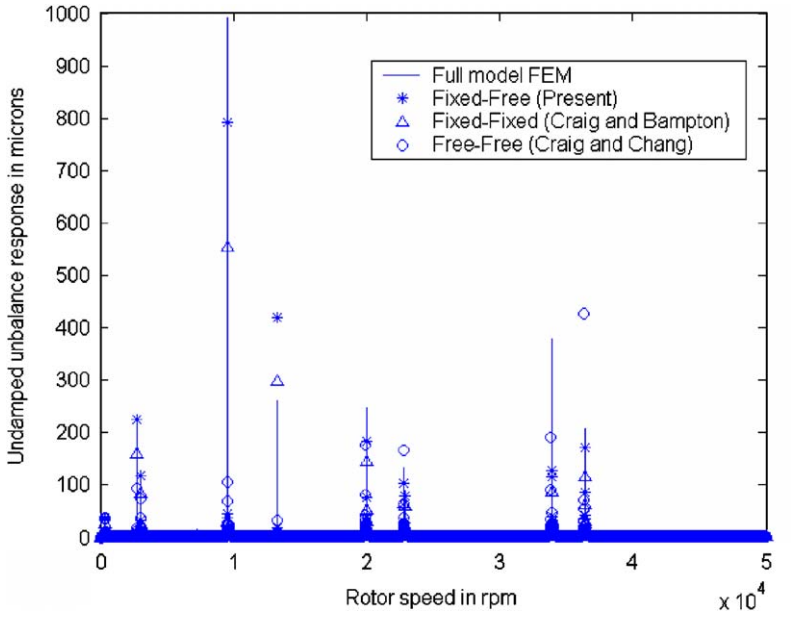

Fig. 6. Undamped unbalance response of cantilever rotor at disc end with 50% of the modes included.

very high spin speed of 100,000 rev/min. It can be seen from Table 1 that only for the 10th forward mode significant error occurs. For lower speeds, the errors occur only at higher modes. Hence, one can neglect the gyroscopic matrix while forming the truncation set. Hence one can adopt a modal matrix based on inertia and stiffness matrix to truncate the gyroscopic matrix.

The cantilever rotor has been divided into two sub-rotors (components each with 20 dof) as shown in Fig. 1 and solved for whirl frequency and unbalance response analysis using fixed-free (present formulation), fixed–fixed (Craig–Bampton) and free–free (Craig–Chang) CMS methods for various levels of modal truncation. The results obtained are compared with a full order FEM. Table 2 gives the comparative results

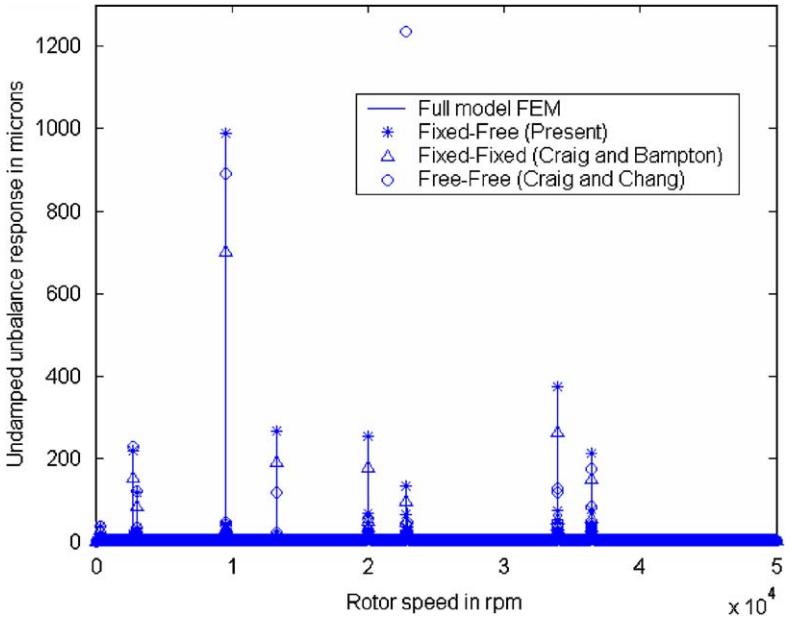

Fig. 7. Undamped unbalance response of cantilever rotor at disc end with 80% of the modes included.

Table 3
Data for the twin spool-rotor of Fig. 2 ($\rho = 7840\,kg/m^3$, $E = 2.07E11\,N/m^2$, $I_P = 2I_D$)

Node	Axial distance (mm)	Inner diameter (mm)	Outer diameter (mm)	Bearing		Disc	
				Stiffness (N/m) $K_{xx} = K_{yy}$	Damping (Ns/m) $C_{xx} = C_{yy}$	Mass (kg)	I_P (kg/mm^2)
1	0	30.4	0	2795E6	5260		
2	76.2	30.4	0			4.904	0.02712
3	254	30.4	0				
4	406.4	30.4	0	8.7598E6			
5	457.2	304	0			4.203	0.02034
6	508	30.4	0	17.519E6	3507		
7	152.4	50.8	38.1	17.519E6	3507		
8	203.2	50.8	38.1			3.327	0.01469
9	355.6	50.8	38.1			2.227	0.09720
10	406.4	50.8	38.1	8.7598E6			

with 50% modal truncation at component level. The present formulation shows excellent convergence and accuracy, when compared to Craig–Bampton or Craig–Chang methods. Campbell diagrams (Figs. 3 and 4) are plotted until rotor speeds of 50,000 rev/min, which include first six backward and forward whirl modes. In Fig. 4, six modes are used for each component (30% modes), while in Fig. 5 the results are for 10 modes for each component (50% modes). It can be observed from these figures that the present method is as good as Craig–Bampton method and far superior to Craig–Chang method as far as whirl frequency analysis is concerned. The present method, it must be emphasized, has the advantage of being easily adapted to carry out non linear analysis unlike the Craig–Bampton method.

Unbalance response analysis is carried out on the first rotor using full model FEM and the results of this is compared with the results obtained using all the above CMS methods with various levels of modal truncation at the component level. The comparisons are given in the Figs. 6 and 7. It can be observed from these results that the present method gives better results with better convergence (as the percentage of modes included is

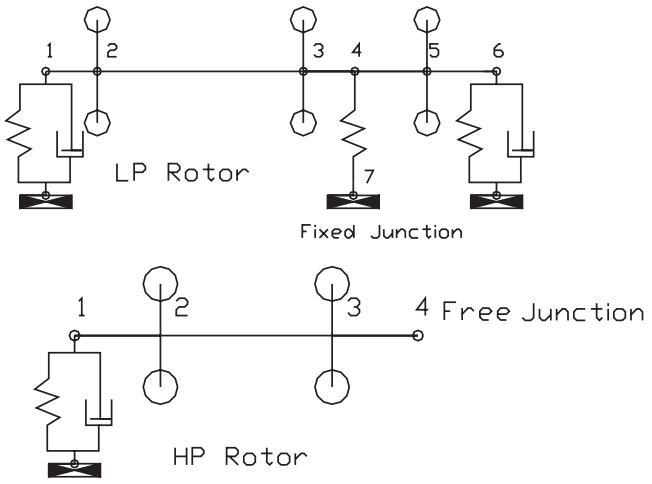

Fig. 8. FEM model of twin-spool aero-engine for fixed–free CMS.

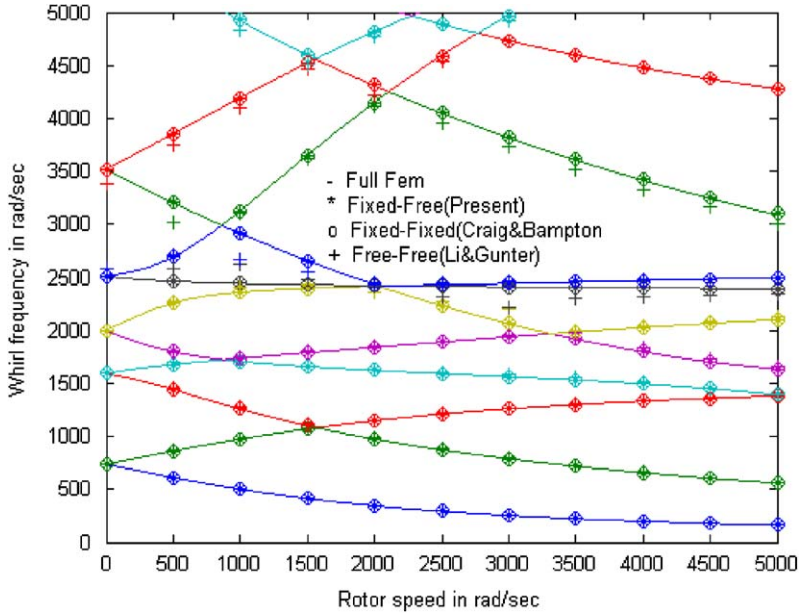

Fig. 9. Whirl frequency analysis of twin-spool rotor model (Fig. 2) with 12 LP and eight HP modes included.

increased). This shows that the present formulation is better for both whirl frequency analysis (free vibration) and forced response analysis.

The second rotor example has also been analyzed for both whirl frequency and unbalance response analysis with damping included. This twin-spool rotor is divided into LP and HP components as shown in Fig. 2. Table 3 shows the rotor properties used in the analysis while Fig. 8 shows the FEM model. The LP rotor has 24 dof (six elements) and the HP rotor 16 DOF (four elements). This rotor is first analyzed for whirl frequency analysis using full order FEM and these results are compared with those obtained from the present formulation, Craig–Bampton and Li–Gunter CMS methods with various levels of modal truncation at the component level. These results are given in Figs. 9 and 10, which show that both the present formulation and the Craig–Bampton method give accurate results while the Li–Gunter method is not as accurate. The convergence of whirl frequencies at speeds of 20,000 and 30,000 rev/min using the present method for various

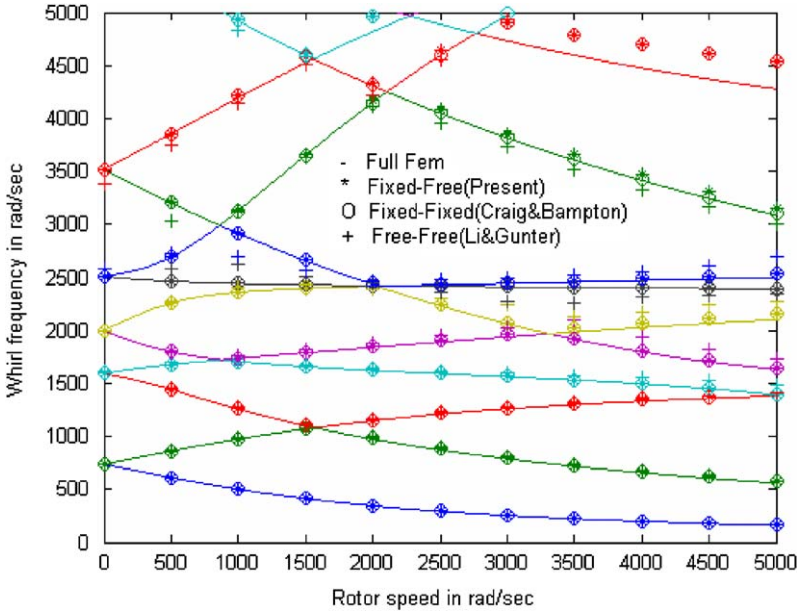

Fig. 10. Whirl frequency analysis of twin-spool rotor model (Fig. 2) with eight LP and six HP modes included.

Table 4
Convergence of rotor whirl frequencies, in rad/s, at a rotor speed 20,000 rev/min for the twin-spool aero-engine example

Mode no.	LP = 8 modes HP = 6 modes	LP = 14 modes HP = 10 modes	LP = 24 modes HP = 10 modes	FEM 40 modes	% Error with (8,6)
λ_{-1}	3.36995E2	3.45326E2	3.45326E2	3.44879E2	2,286
λ_{1}	9.79896E2	9.75388E2	9.75387E2	9.74563E2	0.547
λ_{-2}	1.16110E3	1.14668E3	1.44668E3	1.14721E3	1.210
λ_{2}	1.84173E3	1.83941E3	1.83941E3	1.83961E3	0.115
λ_{-3}	1.62705E3	1.62368E3	1.62368E3	1.62351E3	0.218
λ_{3}	2.37694E3	2.41569E3	2.41569E3	2.41579E3	1.608
λ_{-4}	2.41830E3	2.41865E3	2.41864E3	2.41853E3	0.009
λ_{4}	4.13771E3	4.14242E3	4.14242E3	4.15019E3	0.300
λ_{-5}	2.46954E3	2.43579E3	2.43573E3	2.43571E3	1.388
λ_{5}	4.33272E3	4.31630E3	4.31630E3	4.30914E3	0.547

Table 5
Convergence of rotor whirl frequencies, in rad/s, at a rotor speed of 30,000 rev/min for the twin-spool aero-engine example

Mode no.	LP = 8 modes HP = 6 modes	LP = 14 modes HP = 10 modes	LP = 24 modes HP = 10 modes	FEM 40 modes	% Error with (8,6)
λ_{-1}	2.55790E2	2.54243E2	2.54243E2	2.53847E2	0.765
λ_{1}	1.28741E3	1.25973E3	1.25973E3	1.26031E3	2.150
λ_{-2}	7.96951E2	7.89060E2	7.89055E2	7.88578E2	1.061
λ_{2}	1.94705E3	1.93835E3	1.93835E3	1.93861E3	0.435
λ_{-3}	1.57455E3	1.56345E3	1.56345E3	1.56315E3	0.729
λ_{3}	2.45364E3	2.44366E3	2.44366E3	2.44382E3	0.401
λ_{-4}	2.02592E3	2.06325E3	2.06316E3	2.06304E3	1.799
λ_{4}	4.90102E3	4.73541E3	4.73539E3	4.73464E3	3.514
λ_{-5}	2.42955E3	2.41056E3	2.41056E3	2.41052E3	0.789
λ_{5}	4.99523E3	4.95788E3	4.95785E3	4.97039E3	0.499

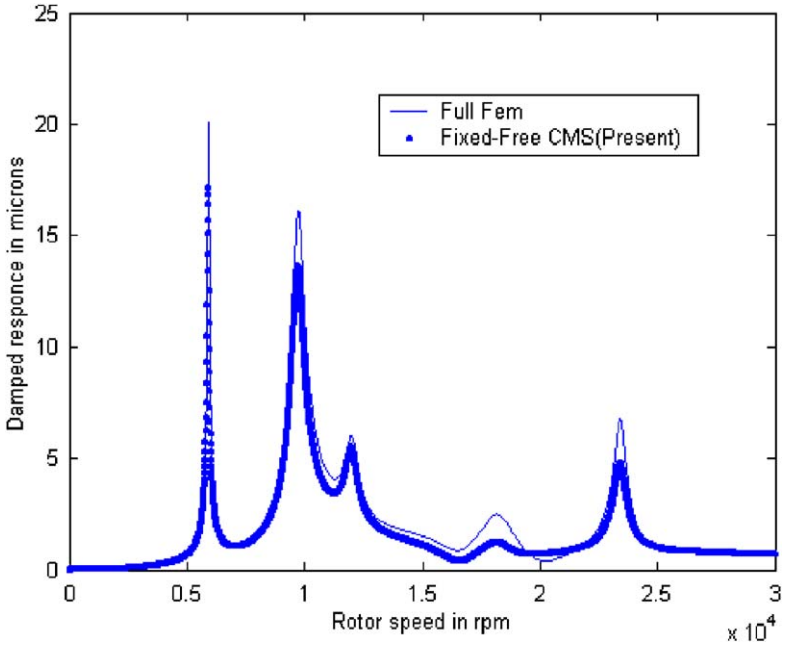

Fig. 11. Damped unbalance response of twin-spool rotor example at the first disc using 12 LP and eight HP modes.

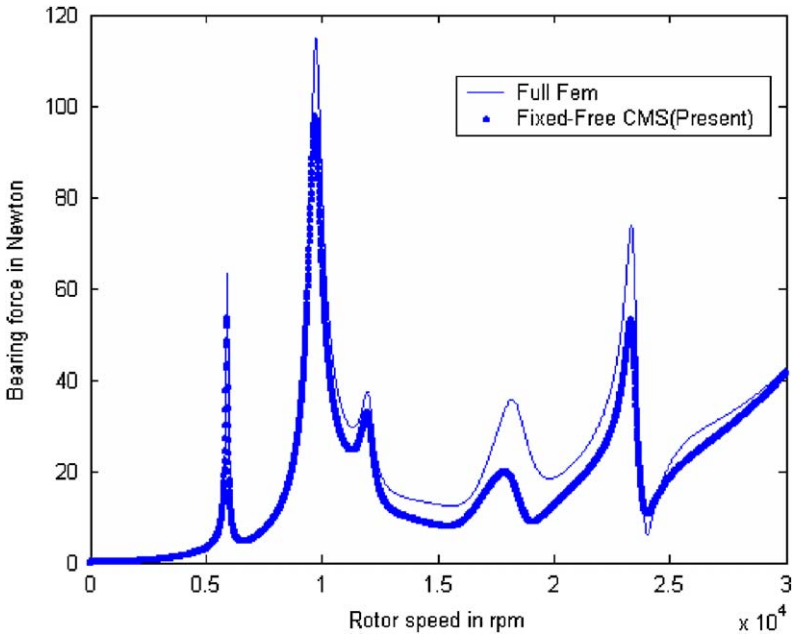

Fig. 12. Force on bearing four of the twin-spool rotor using 12 LP and eight HP modes.

numbers of truncated modes is presented in Tables 4 and 5. This demonstrates that the present formulation is quite accurate. Further, damped unbalance response of this rotor at two locations have been compared with full order FEM. Fig. 11 shows the response of disc #1 while the bearing force on the front bearing has also been calculated in Fig. 12 from the displacements. As expected, the errors show up for the higher modes, which can be corrected by using more component modes.

4. Conclusions

In this paper, a hybrid fixed–free interface method using component modes obtained neglecting the gyroscopic matrix has been developed. The model has been applied to two rotor examples and results compared with fixed–fixed and free–free methods. It has been clearly demonstrated that the present method has much better accuracy and converges better than the traditional CMS methods. Further, there is a choice for the analyst in deciding which junction is to be fixed and which one is to be free, in order to achieve the full potential of this method. In general, the component, which has a minimum number of junction coordinates when compared to interior coordinates is often the best choice to be fixed and the component, which has considerable number of junction coordinates when compared to interior coordinates, is to be kept free. The inherent advantage of this method is that the necessity of treating rigid body modes is eliminated by proper choice of junction coordinate treatment. In this method, all the junction coordinates are kept as physical coordinates, which has advantages for the nonlinear analysis when squeeze film dampers are used.

References

[1] H.D. Nelson, Rotordynamic modelling and analysis procedures: a review, *JSME International Journal, Series C* 41 (1998) 1–12.
[2] W.C. Hurty, J.D. Collins, G.C. Hart, Dynamic analysis of large structures by modal synthesis techniques, *Computers and Structures* 1 (1971) 535–563.
[3] R.R. Craig Jr., M.C.C. Bampton, Coupling of substructures for dynamic analysis, *AIAA Journal* 6 (1968) 1313–1319.
[4] W.C. Hurty, Dynamic analysis of structural systems using component modes, *AIAA Journal* 3 (1965) 678–685.
[5] R. R. Craig Jr., C-J. Chang, On the use of attachment modes in substructure coupling for dynamic analysis, AIAA/ASME 18th Structures, Structural Dynamics and Material Conference, San Diego, CA, 1977.
[6] D.F. Li, E.J. Gunter, Component Mode Synthesis of large rotor systems, *ASME Journal of Engineering for Power* 104 (1982) 552–560.
[7] A. Glasgow, H.D. Nelson, Stability analysis of rotor bearing systems using component mode synthesis, *ASME Journal of Mechanical Design* 102 (1980) 352–359.
[8] L. Meirovitch, A new method of solution of the eigenvalue problem for gyroscopic systems, *AIAA Journal* 12 (1974) 1337–1342.
[9] H.D. Nelson, J.M. McVaugh, The dynamics of rotor-bearing systems using finite elements, *ASME Journal of Engineering for Industry* 106 (1976) 593–601.